DRAFT VERSION NOVEMBER 2, 2004
Preprint typeset using LaTeX style emulateapj v. 11/12/01

THE IMPACT OF SMALL-SCALE STRUCTURE ON COSMOLOGICAL IONIZATION FRONTS AND REIONIZATION

ILIAN T. ILIEV[1], EVAN SCANNAPIECO,[2] AND PAUL R. SHAPIRO[3]
Submitted to ApJ

ABSTRACT

The propagation of cosmological ionization fronts during the reionization of the universe is strongly influenced by small-scale gas inhomogeneities due to structure formation. These inhomogeneities include both collapsed minihalos, which are generally self-shielding, and lower-density structures, which are not. The minihalos are dense and sufficiently optically-thick to trap intergalactic ionization fronts, blocking their path and robbing them of ionizing photons until the minihalo gas is expelled as an evaporative wind. The lower-density structures do not trap these fronts, but they can slow them down by increasing the overall recombination rate in the intergalactic medium (IGM). In this paper we study the effects of both types of inhomogeneities, including nonlinear clustering effects, and we find that both IGM clumping and collapsed minihalos have significant yet qualitatively different impacts on reionization. While the number density of minihalos on average increases strongly with time, the density of minihalos *inside H II regions around ionizing sources* is largely constant. Thus the impact of minihalos is essentially to decrease the number of ionizing photons available to the IGM at all epochs, which is equivalent to a reduction in the luminosity of each source. On the other hand, the effect of IGM clumping increases strongly with time, slowing down reionization and extending it. Thus while the impact of minihalos is largely degenerate with the unknown source efficiency, IGM clumping can help significantly in reconciling the recent observations of cosmic microwave background polarization with quasar absorption spectra at $z \sim 6$, which together point to an early but extended reionization epoch.

Subject headings: hydrodynamics—radiative transfer—galaxies: halos—galaxies: high-redshift—intergalactic medium—cosmology: theory

1. INTRODUCTION

Recent polarization observations of the cosmic microwave background by the *Wilkinson Microwave Anisotropy Probe* (WMAP) imply that reionization was fairly advanced at $z_{\rm re} \sim 15$ (Kogut et al. 2003). This came as a surprise. The prior detection of the Gunn-Peterson effect in the spectra of high-redshift quasars had suggested that reionization was only just ending at $z \sim 6$ (White et al 2003; Fan et al. 2004). That was consistent with predictions of the most accurate numerical simulations in the current ΛCDM paradigm, which had all predicted this transition at $z_{\rm re} \lesssim 8-10$ (Ciardi et al. 2000; Gnedin 2000; Razoumov et al. 2002; Ciardi et al. 2003). Despite many poorly understood details concerning the star formation rate, the escape fraction of ionizing radiation, and the differences in numerical treatments of reionization, $z_{\rm re} \sim 15$ had seemed unlikely, and such an extended period of reionization, impossible.

Now the race is on to reconcile the early onset of reionization suggested by WMAP with the high-redshift Gunn-Peterson effect, which implies neighboring ionized patches finally grew to overlap at $z \sim 6$ (Haiman & Holder 2003; Cen 2003; Wyithe & Loeb 2003; Ciardi et al. 2003). One suggestion is that the universe had two reionization epochs but recombined in between (Cen 2003), yet this ignores the unavoidable spread in redshifts intrinsic to any such IGM transition (Scannapieco, Schneider, & Ferrara 2003; Barkana & Loeb 2004). Other suggestions involve fine-tuning the ionizing photon emissivity for different source halo masses, the escape fraction, and the (possibly metalicity-dependent) Initial Mass Function (IMF), in ways intended to accelerate early ionization, to build up a large enough $\tau_{\rm es}$, but slow down late ionization, to delay the final overlap until $z \approx 6$ (Wyithe & Loeb 2003; Ciardi et al. 2003). Finally, several authors have explored the possibility of early partial reionization due to a decaying particle (Chen & Kamionkowski 2004; Hansen & Haiman 2004), complemented by later full reionization from astrophysical sources.

The role of small-scale inhomogeneities as sinks of ionizing photons has mostly been ignored in this context. Nevertheless, over a large range of redshifts, the recombination time $t_{\rm rec}$ at the mean IGM density is on the order of the corresponding Hubble time, as illustrated in Figure 1. Thus the absorption of ionizing photons during reionization happens predominantly in overdense regions. In hierarchical models like Cold Dark Matter (CDM), the smallest structures are the first to collapse gravitationally and dominate the photon consumption both during the ionization of a region and afterwards, while balancing recombinations.

When the first sources turned on, they ionized the neutral, opaque IGM around them by propagating weak R-type ionization fronts (I-fronts). This type of front moves outward supersonically with respect to both the neutral gas in front of it and the ionized gas behind it, so it races ahead of the hydrodynamical response of the IGM. This process was first described by Shapiro (1986) and Shapiro & Giroux (1987), who solved analytically for the time-varying radius of a spherical I-front surrounding a point source in the expanding IGM and then used this solution to determine when H II regions would grow to the point of overlap, thereby completing reionization. In this study the effect of density inhomogeneity on the motion of the I-front was described by a mean gas clumping factor $C \equiv \langle n^2 \rangle / \langle n \rangle^2$. A clumpy gas has $C > 1$, which causes the ionized gas to re-

[1] Canadian Institute for Theoretical Astrophysics, University of Toronto, 60 St. George Street, Toronto, ON M5S 3H8, Canada
[2] Kavli Institute for Theoretical Physics, Kohn Hall, UC Santa Barbara, Santa Barbara, CA 93106
[3] Department of Astronomy, University of Texas, Austin, TX 78712-1083

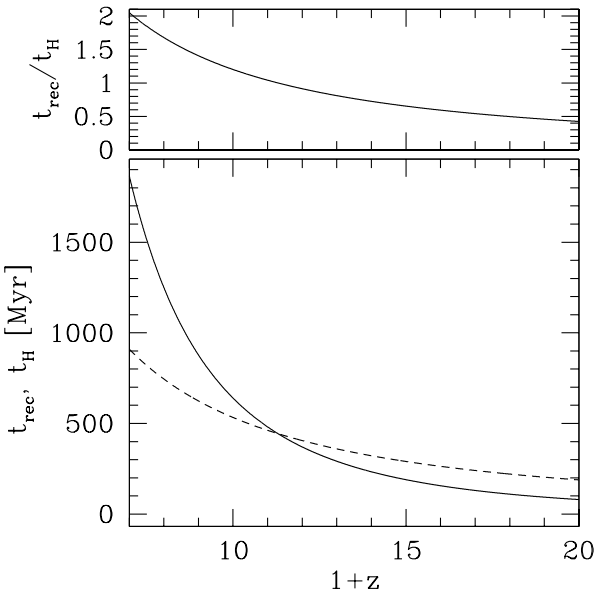

FIG. 1.— Timescales. Hubble time t_H (dashed line) and recombination time $t_{\rm rec} = (\alpha_B n_H)^{-1}$ at the mean IGM density (solid line) vs. redshift z (lower panel) and the ratio of these timescales (top panel).

combine more frequently, increasing the opacity of the H II region to ionizing photons, which reduces the flux reaching the I-front and slows it down. This approach has formed the basis for many more recent semi-analytical treatments of reionization (e.g. Haiman & Holder 2003; Wyithe & Loeb 2003; Venkatesan, Tumlinson, & Shull 2003). The idea that reionization proceeded by the propagation of weak, R-type I-fronts which move too fast to be affected by the gas dynamical disturbance they create is also the basis for most of the *numerical* simulations of reionization carried out to date (e.g. Razoumov et al. 2002; Ciardi, Ferrara, & White, 2003; Sokasian et al. 2004). In particular, all numerical studies that add radiative transfer to a precomputed inhomogeneous cosmological density field (i.e. the "static" limit) are assuming that there is no significant back reaction on the gas[4].

The assumption of either a mean clumping factor or the static limit to model the effect of density inhomogeneity on cosmological I-fronts is not correct even on average, however, unless the clumps are either optically thin or absorb only a small fraction of the ionizing flux. If a clump is self-shielding, then the I-front that encounters it will not remain a weak R-type front if the size of the clump is larger than its Strömgren length (i.e. the length of a column of gas within which the unshielded arrival rate of ionizing photons just balances the recombination rate). In that case the denser gas of the clump must slow the I-front down enough that the disturbed gas inside the clump catches up to the I-front and affects its progress. This transforms the I-front from supersonic, R-type, to subsonic, D-type and "traps" the I-front inside the clump (Shapiro, Iliev & Raga 2004). If the clump is gravitationally bound before the arrival of the I-front, then the I-front will expel the gas from the clump as a supersonic evaporative wind, as long as the clump cannot bind photoionized gas with $T \geq 10^4$ K.

The impact of small-scale inhomogeneities on the global I-fronts that reionized the universe depended upon the relative importance of unshielded and shielded overdense regions and their sizes, densities, and abundances. These IGM inhomogeneities can be divided into two major types, both of which have been modeled only crudely in the majority of reionization studies. Pre-virialized objects, such as filaments and still-collapsing halos, are usually described in terms of the mean clumping factor described above. Current semi-analytical models of reionization either assume a constant clumping factor (Cen 2003; Haiman & Holder 2003; Tumlinson, Venkatesan & Shull 2004), a clumping factor derived from linear theory (Miralda-Escudé, Haehnelt & Rees 2000; Chiu, Fan & Ostriker 2003; Wyithe & Loeb 2003), or ignore clumping altogether (i.e. assume $C = 1$) (Onken & Miralda-Escudé 2004). In practice all these approaches are over-simplified since the clumping factor of the IGM gas is dominated by the highly-overdense nonlinear regions and evolves strongly with redshift.

Modeling of virialized inhomogeneities in previous studies has been even more approximate. An important dividing line that separates two distinct populations of virialized halos is that defined by the virial temperature, $T_{\rm vir} = 10^4 K$. In order for stars to form inside halos, the gas must cool below the virial temperature to become self-gravitating and gravitationally unstable. Radiative cooling in a purely atomic gas of primordial composition is ineffective below $10^4 K$, however, so "minihalos"–halos in the mass range $10^4 M_\odot \lesssim M \lesssim 10^8 M_\odot$, with virial temperatures below 10^4 K – are only able to form stars by forming H_2 molecules, which have the potential to cool the gas below the virial temperature, by rotational-vibrational line excitations. The H_2 that forms in minihalos, though, is easily dissociated by UV photons in the Lyman-Werner bands between 11.2 and 13.6 eV, which are produced in abundance by the first stars, long before the ionizing background from such stars is able to reionize a significant fraction of the universe (e.g. Haiman, Rees, & Loeb 1997; Haiman, Abel & Rees 2000; Ciardi et al. 2000). Thus a generic prediction of current structure formation mod-

[4] An exception to this is the code developed in Gnedin (2000) and Ricotti, Gnedin, & Shull (2002), which combines an approximate treatment of radiative transfer with numerical cosmological gas dynamics.

els is a large population of minihalos that are unable to cool and form stars.

In that case, the dominant source of photons for reionization would have been the more massive halos (i.e. $M \gtrsim 10^8 M_\odot$) with $T_{\rm vir} \geq 10^4 K$, in which atomic line cooling is efficient enough to enable stars to form. From the point of view of such a source halo, all lines of sight will intersect a minihalo at a distance less than the mean spacing between sources (Haiman, Abel & Madau 2001; Shapiro 2001; Shapiro, Iliev, Raga & Martel 2003; Shapiro, Iliev & Raga 2004). Thus, the intergalactic I-fronts must have found their paths blocked by minihalos in every direction, which trapped the fronts until the minihalos were evaporated.

In Shapiro, Iliev & Raga (2004) and Iliev, Shapiro & Raga (2004), we used high-resolution numerical gas dynamical simulations with radiative transfer to study the encounter between an intergalactic I-front and a minihalo in detail, for a wide range of conditions expected during reionization. These results yielded the number of ionizing photons absorbed per minihalo atom during the time between the arrival of the I-front and the evaporation of the minihalo gas, ξ, as a function of the minihalo mass, source flux level and spectrum, and the redshift of the encounter. This a fundamental ingredient we will need here to determine how the presence of minihalos affected global reionization.

This trapping of intergalactic I-fronts by minihalos, combined with the increased recombination rate inside already ionized regions due to small-scale clumping outside the minihalos, may help to explain how reionization could have started early and ended late. As the global I-fronts advanced into fresh neutral regions, they generally encountered minihalos that formed at the *unfiltered* (i.e. not affected by any radiation feedback) rate of the universe without reionization. The mass fraction collapsed into minihalos in such regions grew over time, from 8% to 24% to 31% from $z = 15$ to 9 to 6, so the average number of extra photons consumed per atom by photoevaporation must also have increased with time. This may have enabled minihalos to slow the advance of the global I-fronts, with increasing effect toward late times. Reionization simulations by Ciardi et al. (2003) for example, which neglected minihalos, found that if one assumes a high escape fraction of ionizing photons from the source halos, then the large value of electron scattering optical depth, $\tau_{\rm es}$ observed by WMAP can be achieved by the first stars in galaxies with mass $M \gtrsim 10^9 M_\odot$ as sources. However, in this case, reionization is completed far too early. Minihalos may have the potential to reconcile this discrepancy, increasing the duration of the epoch of reionization and allowing for a similar high value of $\tau_{\rm es}$, while postponing the redshift of overlap.

In this paper, we consider the impact of both minihalos and more general IGM clumping in detail, and attempt to quantify their effects on the duration of the reionization epoch. Driven by measurements of the cosmic microwave background, the number abundance of galaxy clusters, and high redshift supernova distance estimates (e.g. Spergel et al. 2003; Eke, Cole & Frenk 1996; Perlmutter et al. 1999) we focus our attention on the ΛCDM cosmological model with parameters $h = 0.7$, $\Omega_0 = 0.3$, $\Omega_\Lambda = 0.7$, $\Omega_b = 0.05$, $\sigma_8 = 0.87$, and $n_p = 1$, where Ω_0, Ω_Λ, and Ω_b are the total matter, vacuum, and baryonic densities in units of the critical density ($\rho_{\rm crit}$), σ_8^2 is the variance of linear fluctuations filtered on the $8h^{-1}$Mpc scale, and n_p is the index of the primordial power spectrum. The Eisenstein & Hu (1999) transfer function is used throughout.

The structure of this work is as follows. In §2 we generalize the approach of Shapiro & Giroux (1987) to account for the effect of minihalo evaporation on the time-varying radius of a spherical I-front. This will require us to calculate the statistically biased abundance of minihalos at the location of the front and incorporate the simulation results for the ionizing photon consumption rates per minihalo. In §3 we model the global progress of reionization by summing the results from Section 2 over a statistical distribution of source halos, leading to the eventual overlap of neighboring H II regions and the completion of reionization. Our results and conclusions are given in § 4.

2. THE PROPAGATION OF A COSMOLOGICAL IONIZATION FRONT ABOUT A SINGLE SOURCE

2.1. *Cosmological Ionization Fronts in a Clumpy IGM*

When a source of ionizing radiation turns on in the expanding, neutral IGM, a weak, R-type I-front propagates outward. If the IGM were static, this front would decelerate continuously from the moment of turn on, until, within a time comparable to the recombination time, it almost reached the size of the Strömgren sphere. This Strömgren sphere is just large enough that the total recombination rate of ionized atoms inside it equals the ionizing photon luminosity of the central source. At this point the I-front drops to the R-critical speed of twice the sound speed of the ionized gas, and the front transforms from R-type to D-type, preceded by a shock. Thereafter the I-front is affected by the dynamical response of the IGM.

This is not the case, however, in the expanding, average IGM. Shapiro & Giroux (1987) showed that, while it is formally possible to define an "instantaneous" Strömgren radius (which grows in time in proportion to the cosmic scale factor), the actual I-front generally does not reach this radius. Instead, the I-front remains a weak R-type front as long as the source continues to shine, and it would not be correct, therefore, to describe the cosmological H II region as a Strömgren sphere, a misnomer which unfortunately appears in the literature of reionization.

We shall follow the approach of Shapiro & Giroux (1987), in which the H II region is bounded by an I-front whose speed is determined by the I-front continuity jump condition, which balances the outward flux of ionizing photons against the inward flux of newly created ions. The flux that reaches the front will be determined by solving the equation of transfer between the source and the front. We will assume that the IGM is spherically symmetric outside the source. For simplicity the I-fronts are taken to be "sharp", i.e. the width of the transition between the ionized region inside and the neutral region outside the front is small compared to its radius. The actual width is comparable to the absorption mean free path on the neutral side. This assumption of small mean free path is generally a good approximation for a "soft" Population II (Pop. II) stellar spectrum where most ionizing photons have energies near the ionization threshold of hydrogen, for which the absorption cross-section due to neutral hydrogen is large. However, I-fronts are somewhat wider for "hard" spectra like those expected for massive Population III (Pop. III) stars and the power-law spectra of QSOs. In these cases a larger fraction of the ionizing photons are at higher energies, corresponding to lower ionization cross-sections of neutral hydrogen and helium, and thus our approximation of sharp I-fronts is less accurate.

Adopting this picture, we consider an ionizing source emit-

ting $\dot{N}_\gamma$ ionizing photons per unit time. We define the comoving radius of the ionized region as $r_I(t)$ and its comoving volume as $V_I = 4\pi r_I^3/3$. We are interested in H II regions that at all times are much smaller than the scale of the current horizon. The jump condition across the I-front is given by a balance of the flux of neutral atoms and photoionizing photons. In the frame of the front, it can be written as

$$n_{H,1}u_1 = \beta_i^{-1}F, \tag{1}$$

where $n_{H,1}$ is the undisturbed hydrogen number density (in proper coordinates) on the neutral side of the front, $u_1 = a(dr_I/dt)$ is the I-front peculiar velocity, $a = 1/(1+z)$ is the scale factor, and β_i is the number of ionizing photons absorbed to create each ionized H atom that emerges on the ionized side. In the absence of minihalos, $\beta_i = \chi_{\rm eff} \equiv 1 + pA({\rm He})$, which corrects for the presence of helium, with $p = 0, 1$ or 2 if He is mostly neutral, singly ionized or doubly ionized after the passage through the front, and $A({\rm He}) = 0.08$ is the He abundance by number with respect to hydrogen. Finally, F is the number flux of ionizing photons at the current position of the I-front,

$$F = \frac{S(r_I,t)}{4\pi a^2 r_I^2}, \tag{2}$$

where $S(r,t)$ is the number of photons emitted by the central source which pass through a sphere of comoving radius r per unit time, given at $r = r_I$ as

$$S(r_I,t) = \dot{N}_\gamma - \frac{4\pi}{3} r_I^3 a^{-3} ({n_H}^0)^2 C \alpha_B \chi_{\rm eff}, \tag{3}$$

i.e. the number of photons emitted by the source per unit time minus the number of recombinations in the current H II region volume. Here C is the volume-averaged clumping factor, $\alpha_B = 2.6\times10^{-13}$ cm^3 s^{-1} is the case B recombination coefficient for hydrogen at 10^4K and $n_{\rm H}^0$ is the comoving number density of hydrogen in present units, $1.87\times10^{-7}(\Omega_b h^2/0.022)$ cm^{-3}. In all cases, it is safe to assume that the H II regions are cosmologically small, and hence no ionizing photons are lost to redshifting below the hydrogen ionization threshold.

Combining equations (1) - (3), the evolution of the comoving volume of the ionized region V_I is given by

$$\frac{dV_I}{dt} \equiv 4\pi r_I^2 \frac{dr_I}{dt} \equiv \frac{1}{\chi_{\rm eff} n_H^0}\dot{N}_\gamma - \alpha_B C (1+z)^3 n_H^0 V_I. \tag{4}$$

Defining

$$V_{\rm S,i} = \frac{4\pi r_{\rm S,i}^3}{3} = \frac{\dot{N}_\gamma}{\chi_{\rm eff}\alpha_B C (n_{\rm H}^0)^2}, \tag{5}$$

we can write equation (4) in dimensionless form

$$\frac{dy}{dx} = 1 - y(1+z)^3, \tag{6}$$

where $y \equiv V_I/V_{\rm S,i} = (r_I/r_{\rm S,i})^3$, $x \equiv t/t_1$ and $t_1 = 1/(\alpha_B C n_{\rm H}^0)$ is the recombination time of the mean IGM at present (Shapiro & Giroux 1987).

If we define $d\tau = dx/a^3 = (1+z)^3 dx$, equation (6) becomes

$$\frac{dy}{d\tau} = (1+z)^{-3} - y, \tag{7}$$

for which a formal solution is

$$y(t) = e^{-\tau(t)} \int_{\tau(t_i)}^{\tau(t)} d\tau' \frac{e^{\tau'}}{[1+z(\tau')]^3}, \tag{8}$$

where t_i is the time of source turn-on and for the flat, ΛCDM model

$$\frac{d\tau}{dz} = -\frac{(1+z)^2}{H_0 t_1 [\Omega_0 (1+z)^3 + \Omega_\Lambda]^{1/2}}. \tag{9}$$

Equation (9) has a solution

$$\tau(z) = \kappa \left\{ 1 - \left[\Omega_0 (1+z)^3 + \Omega_\Lambda\right]^{1/2} \right\}, \tag{10}$$

where $\kappa \equiv \frac{2}{3H_0 t_1 \Omega_0}$ and the arbitrary constant of integration is chosen so that $\tau(z=0) = 0$. At high redshift, before and during reionization, we have $\Omega_0 >> \Omega_\Lambda/(1+z)^3$ and the solution (10) becomes

$$\tau(z) = \kappa[1 - \Omega_0^{1/2}(1+z)^{3/2}]. \tag{11}$$

In this limit equation (8) simplifies to

$$y(t) = \Omega_0 \kappa^2 e^{-\tau(t)} \int_{\tau(t_i)}^{\tau(t)} d\tau' \frac{e^{\tau'}}{(\kappa - \tau')^2}. \tag{12}$$

Equation (12) has an exact analytical solution given by

$$y = \frac{\eta}{(1+z_i)^3} e^{\eta t_i/t} \left[\frac{t}{t_i} Ei(2, \eta\frac{t_i}{t}) - Ei(2,\eta) \right], \tag{13}$$

where $\eta \equiv 2(1+z_i)^{3/2}/(3H_0 t_1 \Omega_0^{1/2})$ and $Ei(2,x) \equiv \int_1^\infty \frac{e^{-xt}}{t^2} dt$ is the Exponential integral of second order. The solution in equation (13) reduces to the one in equation (10a) of Shapiro & Giroux (1987) for a flat, matter-dominated universe with $\Omega_0 = 1$, $t = 2/(3H)$, and thus $\eta = (1+z_i)^3 t_i/t_1$.

2.2. *The Average Effect of Minihalo Evaporation on Cosmological Ionization Front Propagation*

Having outlined a formalism to describe the expansion of ionization fronts in a ΛCDM cosmology, we next address the question of absorption by minihalos. As described in §1, when an intergalactic I-front encounters an individual minihalo, it is trapped until the minihalo gas is evaporated. For every minihalo atom, this process consumes ξ ionizing photons. Suppose we consider the average effect of this process on the global I-front which moves through a medium comprised of minihalos embedded in the IGM. The average speed throughout this compound medium will be given by a modified I-front continuity jump condition which takes account of the additional photon consumption due to minihalos. In particular, the quantity β_i in eq. (1) should now be replaced by the following

$$\beta_i \equiv (1 - f_{\rm coll})\chi_{\rm eff} + [1 + A({\rm He})] f_{\rm coll,MH} \bar{\xi}, \tag{14}$$

where $f_{\rm coll}$ is the total collapsed baryon fraction (i.e. over *all* halo masses) and $f_{\rm coll,MH}$ is the collapsed fraction of just the minihalos. Finally, if ξ is the the number of ionizing photons consumed per minihalo atom in the encounter between the intergalactic I-front and an individual minihalo, then $\bar{\xi}$ is the appropriate average over the distribution of minihalos at the instantaneous location of the global I-front. Inserting eq. (14) into eq. (1) then yields

$$n_{H,1}u_1 = \frac{F}{(1 - f_{\rm coll})\chi_{\rm eff} + [1 + A({\rm He})] f_{\rm coll,MH}\bar{\xi}}, \tag{15}$$

where $n_{H,1}$ refers to the total H atom density, including both the IGM and all halos.

As usual the flux, F, in this I-front jump condition is determined by integrating the equation of transfer over the ionized region between the source halo and the I-front. By definition, the minihalos originally inside this region do not affect this integration, however, since they will already have been evaporated by the passage of the global I-front, thereby returning their atoms to the IGM inside the H II region. We assume, for simplicity, that the evaporated minihalo gas shares the mean

clumping factor the IGM into which it is mixed. In that case, the flux at the I-front is given by

$$F = \frac{\dot{N}_\gamma - \alpha_B C (1+z)^3 (n_H^0)^2 \chi_{\rm eff} (V_I - V_0)}{4\pi a^2 r_I^2}, \quad (16)$$

where we have been careful now to start our integration of the transfer equation from the Lagrangian volume of the source halo (i.e. a volume which, when multiplied by the mean density, gives the mass of the source halo).

Combining equations (15) and (16), the evolution of the comoving volume of the H II region in the presence of minihalos is then given by

$$\frac{dV_I}{dt} = \frac{1}{\left[(1-f_{\rm coll})\chi_{\rm eff} + [1+A({\rm He})] f_{\rm coll,MH} \bar{\xi}\right]} \times \left[\frac{\dot{N}_\gamma}{n_H^0} - \alpha_B C (1+z)^3 n_H^0 \chi_{\rm eff} (V_I - V_0)\right], \quad (17)$$

where initially $V_I = V_0$. We note that the solutions in §2.1 in the absence of minihalos, including the exact analytical solution for $V_I(t)$ and $r_I(t)$ in equation (13), will be valid here in the presence of minihalos as well, if β_i in equation (14) and the clumping factor C are constants, and t_1 is redefined as

$$t_1 \equiv \left(\alpha_B C n_H^0 \frac{\chi_{\rm eff}}{\beta_i}\right)^{-1}. \quad (18)$$

In general, both β_i and C will not be constant, but nevertheless this limit provides a useful check and some insight, as well shall see below.

We adopt a simple model to account for infall when computing the flux. The radial coordinate, r_I, adopted in our formalism above is essentially a Lagrangian one, in which we have assumed that the local mean density of the gas around the source is equal to the cosmic mean IGM density. In reality, all massive sources are found in overdense regions, due to the gravitational influence on the surrounding gas. We estimate the map between the Lagrangian and Eulerian comoving radii using a simple "top-hat" picture, which is a simplified version of the model described in Barkana (2004).

We compute the cross-correlation between a sphere of Lagrangian radius r_I and spherical perturbation of mass equal to the source halo mass $M_s = (4\pi/3) r_0^3 \Omega_0 \rho_{\rm crit}$ as

$$\sigma^2(r_0, r_I) \equiv \frac{1}{2\pi} \int_0^\infty k^2 dk P(k) W(kr_0) W(kr_I), \quad (19)$$

where $P(k)$ is the initial matter power spectrum, linearly extrapolated to the present, and $W(x)$ is the spherical top-hat window function, defined in Fourier space as $W(x) \equiv 3\left[\frac{\sin(x)}{x^3} - \cos(x)x^2\right]$, where r_0 is the Lagrangian radius of the source itself. Defining $\sigma^2(r_0) \equiv \sigma^2(r_0, r_0)$, the expected value of the linear overdensity of a sphere of Lagrangian radius r_I about the source is then given by

$$\bar{\delta}_L(r_I) = \frac{1.69 D(z)}{D(z_s)} \frac{\sigma^2(r_0, r_I)}{\sigma^2(r_0)} + 1. \quad (20)$$

Here we use $\bar{\delta}_L$ to denote the average density within the sphere, $D(z)$ is the linear growth factor, z_s is the collapse redshift for the halo, and the "+1" appears since we are defining the overdensity as $\rho/\bar{\rho}$ instead of $\rho/\bar{\rho} - 1$. For simplicity, we assume $z = z_s$, i.e. that the growth of the mass after it collapses due to secondary infall, is small.

The linear overdensity $\bar{\delta}_L$ can be related to the corresponding nonlinear overdensity, $\bar{\delta}$, by the standard spherical collapse model (e.g. Peebles 1980). In this case, both quantities can be expressed parametrically, in terms of a "collapse parameter" θ as

$$\bar{\delta} = \frac{9}{2} \frac{(\theta - \sin\theta)^2}{(1-\cos\theta)^3}, \quad (21)$$

and

$$\bar{\delta}_L = \frac{3}{5}\left(\frac{3}{4}\right)^{2/3} (\theta - \sin\theta)^{2/3} + 1. \quad (22)$$

These equations define the relationship between the Eulerian and Lagrangian comoving radii as

$$r_{I,E} = r_I \bar{\delta}(r_I, r_0)^{-1/3}, \quad (23)$$

since $\bar{\delta}$ given by equation (21) above is the average overdensity within an Eulerian sphere of Lagrangian radius r_I.

In the presence of infall, equation (17) becomes

$$\frac{dV_I}{dt} = \frac{1}{\left[(1-f_{\rm coll})\chi_{\rm eff} + [1+A({\rm He})] f_{\rm coll,MH} \bar{\xi}\right]} \times \left[\frac{\dot{N}_\gamma}{n_H^0} - \alpha_B C (1+z)^3 n_H^0 \chi_{\rm eff} \int_{V_{0,E}}^{V_{I,E}} dV'_{I,E} \delta(V'_{I,E})^2\right], \quad (24)$$

where now δ is not the average δ within the sphere, but rather δ at the boundary, and $V_{I,E} \equiv V_I \bar{\delta}^{-1}$ is the Eulerian volume. We compute δ as follows. The comoving volume satisfies:

$$\Delta V_{I,E} \delta(V_{I,E}) + V_{I,E} \bar{\delta}(V_{I,E}) = [V_{I,E} + \Delta V_{I,E}] \bar{\delta}(V_{I,E} + \Delta V_{I,E}), \quad (25)$$

where $\Delta V_{I,E}$ is a small change in the size of the radius. Working to first order in $\Delta V_{I,E}$, this gives

$$\delta = \bar{\delta} + V_{I,E} \frac{d\bar{\delta}}{dV_{I,E}}. \quad (26)$$

We can therefore rewrite equation (24) using the Lagrangian volume as

$$\frac{dV_I}{dt} = \frac{1}{\left[(1-f_{\rm coll})\chi_{\rm eff} + [1+A({\rm He})] f_{\rm coll,MH} \bar{\xi}\right]} \times \left[\frac{\dot{N}_\gamma}{n_H^0} - \alpha_B C (1+z)^3 n_H^0 \chi_{\rm eff} \int_{V_0}^{V_I} dV'_I \delta(V'_I)^{-1} \delta(V'_I)^2\right] \quad (27)$$

The relevant overdensity that appears in equation (27) is

$$\delta_{\rm clump}(V_I) \equiv \frac{1}{V_I - V_0} \int_{V_0}^{V_I} dV'_I \delta(V'_I). \quad (28)$$

In Figure 2, we show $\bar{\delta}$, δ, and $\delta_{\rm clump}$ around peaks of mass $10^8 M_\odot$ and $10^{11} M_\odot$. Note that $\delta_{\rm clump}$ exceeds $\bar{\delta}$ over a range of radii, because $\delta_{\rm clump}$ is an average in Lagrangian coordinates and $\bar{\delta}$ is an average in Eulerian coordinates. Finally, the flux in equation (16) is corrected by a similar factor of $\delta_{\rm clump}$, yielding

$$F = \frac{\dot{N}_\gamma - \alpha_B C (1+z)^3 (n_H^0)^2 \chi_{\rm eff} (V_I - V_0) \delta_{\rm clump}(V_I)}{4\pi a^2 r_{I,E}^2}. \quad (29)$$

The average number of ionizing photons absorbed per minihalo atom, $\bar{\xi}$, in the process of evaporating all the minihalos at the current location of the I-front, $r_I(t)$, must now be specified. Iliev, Shapiro & Raga (2004) have shown that the number of photons per atom absorbed by a minihalo of mass M_7 (in units of $10^7 M_\odot$), overtaken by an intergalactic I-front at a redshift of z which is driven by an external source of flux F_0, the flux in units of that from a source emitting $N_{\rm ph} = 10^{56} {\rm s}^{-1}$ ionizing photons per second at a proper distance d of 1 Mpc, i.e.

$$F_0 \equiv \frac{N_{\rm ph,56}}{d_{\rm Mpc}^2} = \frac{F}{8.356 \times 10^5 {\rm s}^{-1} {\rm cm}^{-2}}, \quad (30)$$

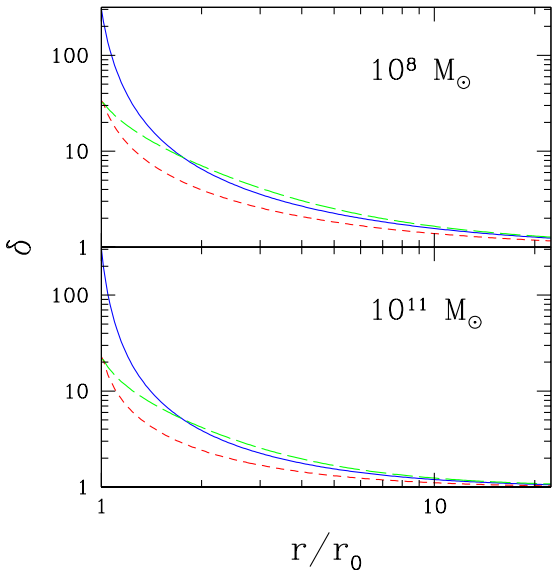

FIG. 2.— Overdensites around a source of a given mass, as labeled, versus Lagrangian distance from the center of the source (in units of the Lagrangian radius of the halo): the mean $\bar{\delta}$ is solid (colored blue in electronic edition), the density at the boundary, δ, is short-dashed (colored red in electronic edition), and $\delta_{\rm clump}$ is long-dashed (colored green in electronic edition). (See the electronic edition of the Journal for the color version of this figure.)

during its photoevaporation is given by

$$\xi(M,z,F_0) \equiv 1+\phi_1(M)\phi_2(z)\phi_3(F_0) \tag{31}$$

where $\phi_1(M) \equiv A(M_7^{B+C\log_{10}M_7})$, $\phi_2(z) \equiv \left[G+H\,(1+z)\,/10\right]$ and $\phi_3(F_0) \equiv F_0^{D+E\log_{10}F_0}$. Here the factors A-G are dependent on the spectrum of the ionizing sources: A = (4.4, 4.0, 2.4), B =(0.334, 0.364, 0.338), C = (0.023, 0.033, 0.032), D =(0.199, 0.240, 0.219), E = (-0.042,-0.021,-0.036), G=(0.,0.,0.1), H=(1, 1, 0.9), for the cases in which the ionizing spectrum is taken to be a 5×10^4K blackbody representing Pop. II stars , a QSO-like power-law spectrum with slope of -1.8, or a 10^5K blackbody representing Pop. III stars, respectively.

In order to use this result in equation (27), the quantity $\xi(M,z,F_0)$ must first be averaged over the mass function of minihalos at $r_I(t)$ on the undisturbed side of the I-front as the H II region evolves with time. Since $\xi(M,z,F_0)$ depends on $F_0(t)$, which also depends on $r_I(t)$ according to equation (29), equations (27) and (29) are coupled and must be solved simultaneously. We shall consider three analytical approximations for the minihalo mass function when averaging $\xi(M,z,F_0)$ to obtain $\bar{\xi}$. The first two approaches, described in § 2.2.1, are based on the well-known Press-Schechter (PS) approximation for the mass function averaged over all space at a given redshift (Press & Schechter 1974). We shall refer to these, which depend upon z and F_0, but not upon $r_I(t)$ or the source halo properties, as "unbiased minihalo" averages. The third approximation, described in § 2.2.2, is based upon an extension of the PS approach which takes account of the spatial correlation between the minihalos and the central source halos, as described by Scannapieco & Barkana (2002). In this last approximation, which we refer to as the "biased minihalo" average, $\bar{\xi}$ not only depends upon z and F_0, but also on $r_I(t)$ and the source halo mass.

2.2.1. *The Average Photon Consumption Rate for Unbiased Minihalos.*

We begin by defining the average photon consumption rate per minihalo atom

$$\bar{\xi}_{\rm nb,1}(z,F_0) \equiv \frac{\int_{M_{\rm min}}^{M_{\rm max}} dM\,\frac{dn(M,z)}{dM}\,M\,\xi(M,z,F_0)}{\int_{M_{\rm min}}^{M_{\rm max}} dM\,\frac{dn(M,z)}{dM}\,M}, \tag{32}$$

where $\frac{dn(M,z)}{dM}$ is the PS mass function of halos, if we assume that the minihalos at a given redshift z just formed at that redshift. If, on the other hand, we assume that minihalos at z had a distribution of formation redshifts z_f, with $z_f \geq z$, then

$$\bar{\xi}_{\rm nb,2}(z,F_0) \equiv \frac{\int_{M_{\rm min}}^{M_{\rm max}} dM\int_z^\infty dz_f\,\frac{dn(M,z_f)}{dMdz_f}\,M\,\xi(M,z_f,F_0)}{\int_{M_{\rm min}}^{M_{\rm max}} dM\int_z^\infty dz_f\,\frac{dn(M,z_f)}{dMdz_f}\,M}. \tag{33}$$

In both these equations, the limit $M_{\rm min}$ is the minimum minihalo mass (which we assume here to be the Jeans mass at that epoch), while $M_{\rm max} = M(T_{\rm vir} = 10^4K)$ is the halo mass at that epoch for which $T_{\rm vir} = 10^4$ K. In equation (33) we have approximately accounted for the distribution of minihalo formation times, by taking the derivative of the mass function, which glosses over the fact that the change in this function at a given mass M includes both a positive contribution from halos whose masses have increased to M from lower values, as well as a negative contribution from halos whose masses have increased from M to higher values. The error introduced by this approximation is small, however (eg. Kitayama & Suto 1996), and is justified given the other uncertainties involved.

2.2.2. *The Average Photon Consumption Rate for Biased Minihalos.*

To calculate the biased distribution of minihalos about a given source, we employ an analytical formalism that tracks the correlated formation of objects. Our approach, described in detail in Scannapieco & Barkana (2002), extends the standard PS method using a simple approximation to construct the bivariate mass function of two perturbations of arbitrary mass and collapse redshift, initially separated by a fixed comoving distance (see also Porciani et al. 1998). From this function we can construct the number density of minihalos of mass M that

form at an initial redshift z at a comoving distance r from the source halo of mass M_s and formation redshift z_s:

$$\frac{dn}{dM}(M,z,r|M_s,z_s) = \frac{\frac{d^2n}{dMdM_s}(M,z,M_s,z_s,r)}{\frac{dn}{dM_s}(M_s,z_s)}, \quad (34)$$

where $\frac{dn}{dM_s}(M_s,z_s)$ is the usual PS mass function and $\frac{d^2n}{dMdM_s}(M,z,M_s,z_s,r)$ is the bivariate mass function that gives the product of the differential number densities at two points separated by an initial comoving distance r, at any two masses and redshifts. Note that this expression interpolates smoothly between all standard analytical limits: reducing, for example, to the standard halo bias expression described by Mo & White (1996) in the limit of equal mass halos at the same redshift, and reproducing the Lacey & Cole (1993) progenitor distribution in the limit of different-mass halos at the same position at different redshifts. Note also that in adopting this definition we are effectively working in Lagrangian space, such that r is the *initial* comoving distance between the perturbations. As a shorthand we define $\frac{dn_{mh,s}}{dM}(z,r) \equiv \frac{dn}{dM}(M,z,r|M_s,z_s)$. With this definition the biased values of the average photon consumption per minihalo atom corresponding to the two unbiased cases in equations (32) and (33), respectively, are

$$\bar{\xi}_{b,1}(z,F_0,r_I,M_s) = \frac{\int_{M_{\rm min}}^{M_{\rm max}} dM\, \frac{dn_{mh,s}}{dM}(z,r_I)\, M\, \xi(M,z,F_0)}{\int_{M_{\rm min}}^{M_{\rm max}} dM\, \frac{dn_{mh,s}}{dM}(z,r_I)\, M} \quad (35)$$

and

$$\bar{\xi}_{b,2}(z,F_0,r_I,M_s) = \frac{\int_{M_{\rm min}}^{M_{\rm max}} dM \int_z^\infty dz_f\, \frac{dn_{mh,s}}{dMdz_f}(z_f,r_I)\, M\, \xi(M,z_f,F_0)}{\int_{M_{\rm min}}^{M_{\rm max}} dM \int_z^\infty dz_f\, \frac{dn_{mh,s}}{dMdz_f}(z_f,r_I)\, M}, \quad (36)$$

with r_I the Lagrangian radius of the I-front.

We can anticipate how important this bias effect is likely to be in determining the average minihalo consumption rate by considering its impact on the minihalo collapsed fraction in the vicinity of a given source halo. In Figure 3, we plot the average (unbiased) minihalo collapsed fraction versus the biased value, which varies with distance from the source halo, for two halo masses $10^8 M_\odot$ and $10^{11} M_\odot$, at redshifts $z = 7$ and $z = 15$. These halo masses and redshifts illustrate the range of behavior expected during reionization. In terms of the Gaussian-random-noise initial conditions for our ΛCDM cosmological model, $10^8 M_\odot$ halos correspond to fluctuations that are 3.2 σ (1.6 σ) at $z = 15$ (7), respectively while $10^{11} M_\odot$ halos are 6.4 σ (3.2 σ) at these same redshifts.

The distance between sources and minihalos is measured in terms of the comoving Lagrangian (i.e. unperturbed) radius of a given mass shell surrounding the central source, in units of r_0, the Lagrangian radius of the source. According to this figure, the bias can be significant for minihalos located in the range $1 \lesssim r/r_0 \lesssim 10$. For typical source halos, in fact, the biased collapsed fraction in the neighborhood of the source hardly declines with increasing redshift, in contrast with the unbiased collapsed fraction which declines by a factor of more than 3 between $z = 7$ and $z = 15$.

2.3. *The Ionizing Photon Luminosity of the Central Source*

The total ionizing photon output of a source, N_γ, and its time evolution depend on the mass of the host halo M_s, photon production per stellar baryon N_i, star-formation efficiency f_* and ionizing photon escape fraction $f_{\rm esc}$. We then define the total ionizing photon output per source atom that escapes the source halo as:

$$f_\gamma = f_* f_{\rm esc} N_i, \quad (37)$$

thus the source emits a total of $N_\gamma = f_\gamma M\Omega_b/(\mu m_p)$ during its lifetime, where μm_p is the mean mass per atom.

The star-formation efficiency f_* and ionizing photon escape fraction $f_{\rm esc}$ are highly uncertain in general, and even more so for the high-redshift galaxies responsible for reionization. Their estimated values vary by several orders of magnitude between different observational and theoretical estimates (Leitherer et al. 1995; Ricotti & Shull 2000; Heckman et al. 2001; Steidel et al. 2001; Tan & McKee 2001). For simplicity, and since the principle aim of this investigation is to show the effect of small-scale structure rather than model the sources in detail, we assume that each source produces a fixed number f_γ of ionizing photons which escape from the source galaxy per atom in the source during the source's lifetime. The ionizing photon production per atom for Pop. II low-metalicity stars with a Salpeter IMF is $N_i = 3000 - 10000$ (Leitherer et al. 1999). Zero-metalicity, massive Pop. III stars, on the other hand, are estimated to produce values of N_i that rise sharply with mass from 25,000 to 80,000 as stellar mass increases from 10 $M_\odot$ to 50 $M_\odot$, then gradually reach a peak of 90,000 at 120 $M_\odot$, and finally decline slowly to 80,000 by 500 $M_\odot$ (Schaerer 2002; Tumlinson, Venkatesan & Shull 2004). While individual Pop. III stars have higher values of f_γ than Pop. II stars of the same mass, a non-trivial part of the increase from Pop. II to Pop. III quoted above reflects the fact that the assumed Pop. II IMF has many low-mass stars, which are inefficient ionizing sources, while the Pop. III IMF is often hypothesized to contain only massive stars.

Assuming, conservatively, that $N_i \geq 4000$ for Pop. II stars and $N_i \geq 25,000$ for Pop. III stars, and taking moderate fiducial values for the photon escape fraction and star formation efficiency of $f_{\rm esc} = 0.1$ and $f_* = 0.1$, yields $f_\gamma \geq (40, 250)(f_{\rm esc}/0.1)(f_*/0.1)$ for (Pop. II, Pop. III), respectively. We shall further assume that the time-dependence of this ionizing photon output is characteristic of a starburst with a photon luminosity

$$\dot{N}_\gamma = f_\gamma \frac{\alpha - 1}{\alpha} \frac{M\Omega_b}{\mu m_p t_s} \times \begin{cases} 1 & t \leq t_s \\ \left(\frac{t}{t_s}\right)^{-\alpha} & t > t_s, \end{cases} \quad (38)$$

where $\alpha = 4.5$, i.e. we assume that the source is steady for a time t_s, after which the photon flux decreases as power of time (Haiman & Holder 2003). Here t_s is the characteristic time for a source to fade, essentially the typical source lifetime. For individual massive stars $t_s \approx 3$ Myr, but starbursts could in principle last significantly longer, thus we consider both the cases $t_s = 3$ Myr and $t_s = 100$ Myr. We assume that the He correction $\chi_{\rm eff}$ is 1.08 for the softer Pop. II spectrum and 1.16 for the harder Pop. III and QSO spectra.

2.4. *Results for Individual H II Regions*

We present the results of our numerical solution of the spherical I-front evolution equations from §2.2 for two illustrative cases. Sample results for two source halos, a $10^8 M_\odot$ halo that turns on at $z = 15$ and a $10^{11} M_\odot$ halo that turns on at $z = 7$, both with $f_\gamma = 250$, $t_s = 3$ Myr, and Pop. II spectra, are given in Figures 4-6. In both cases we display results for a variety of clumping factors ($C = 0, 1, 10$) and successive approximations of no minihalos, unbiased minihalos [as given by eq. (32)], and

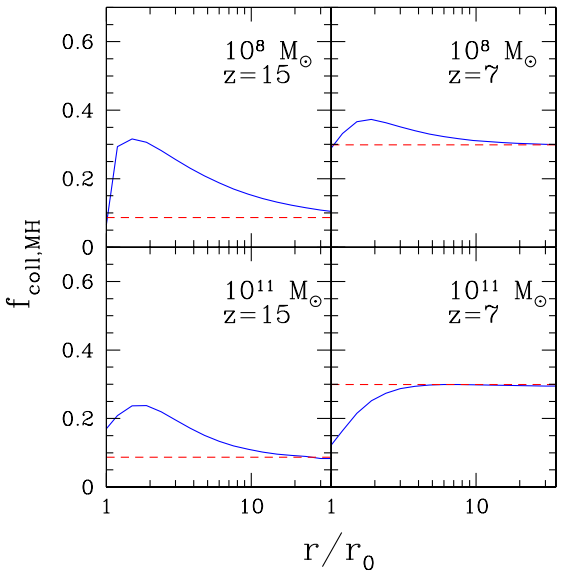

FIG. 3.— Biased collapsed fraction of baryons in minihalos, $f_{\rm coll,MH}$, as a function of the Lagrangian distance from the source halo (in units of the source halo Lagrangian radius) for sources of masses $10^8 M_\odot$ and $10^{11} M_\odot$ and redshifts $z = 15$ and $z = 7$, as indicated (solid). For reference we also show the unbiased collapsed fraction of baryons in minihalos at the corresponding redshifts (dashed).(See the electronic edition of the Journal for the color version of this figure.)

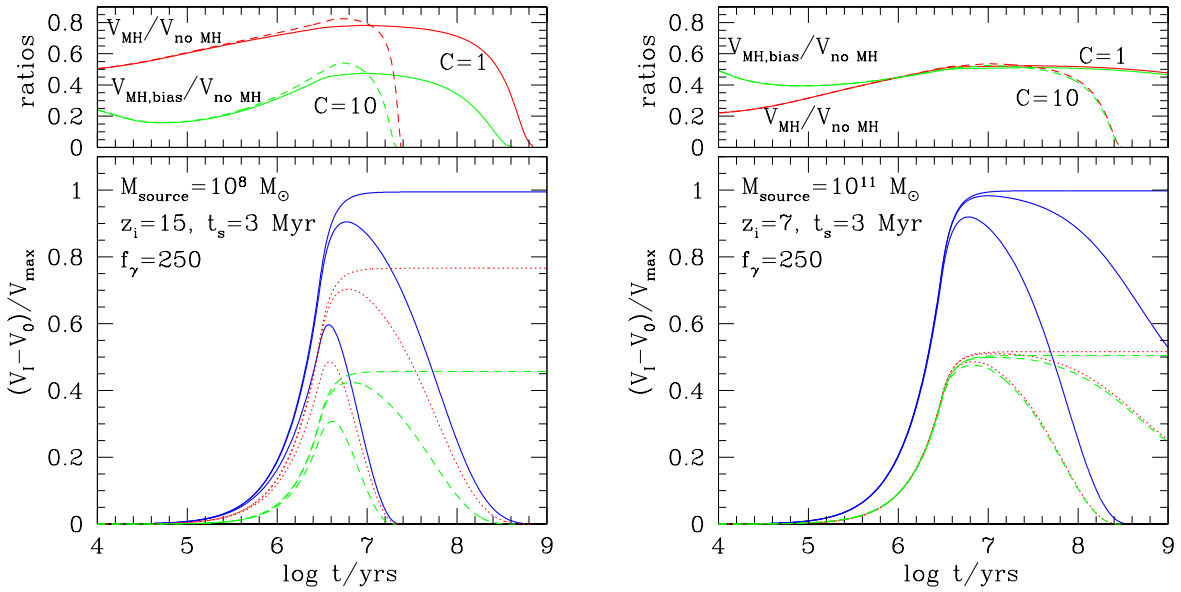

FIG. 4.— *Bottom:* The evolution of the Lagrangian volume of the H II region about a single source of (left) mass $10^8 M_\odot$ that turns on at $z_i = 15$, or (right) mass $10^{11} M_\odot$ that turns on at $z = 7$. Both sources have Pop. II stellar spectra and lifetimes of $t_s = 3$ Myr, during which they produce a total of $f_\gamma = 250$ photons/atom. Shown are the cases of no minihalos (solid), unbiased minihalos (dotted), and biased minihalos (dashed) for IGM clumping factors (top to bottom in each case) $C = 0$ (i.e. no recombinations in IGM gas), 1 (mean IGM), and 10 (clumped IGM). $V_{\rm max}$ is the maximum ionized volume reached during the lifetime of the source in the $C = 0$ case with no minihalos, as defined in the text. *Top:* Ratios of the ionized volumes with unbiased and biased minihalos to the no minihalo case, as labeled, for $C = 1$ (solid) and 10 (dashed).(See the electronic edition of the Journal for the color version of this figure.)

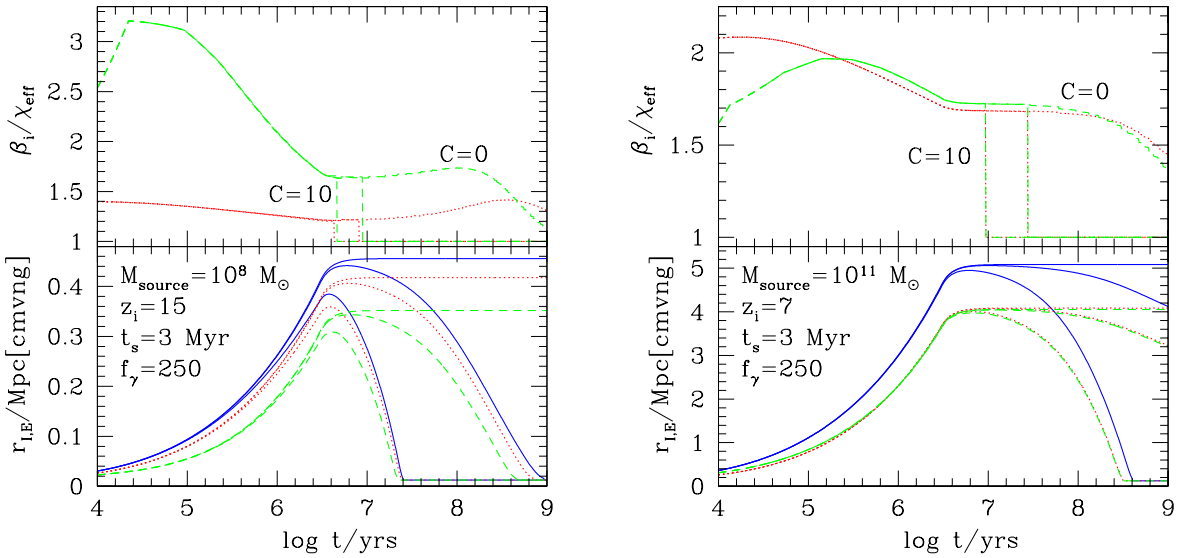

FIG. 5.— Evolution of individual H II regions with the same source parameters as in Figure 4. *Top:* The correction factor $\beta_i/\chi_{\rm eff}$ due to minihalos for the number of ionized photons consumed per atom that crosses the I-front, for biased (dashed) and unbiased minihalos (dotted) for $C = 0, 1$ and 10. *Bottom:* Comoving radius of the H II region for no minihalos (solid), unbiased (dotted) and biased minihalos (dashed) for $C = 0, 1$ and 10. (See the electronic edition of the Journal for the color version of this figure.)

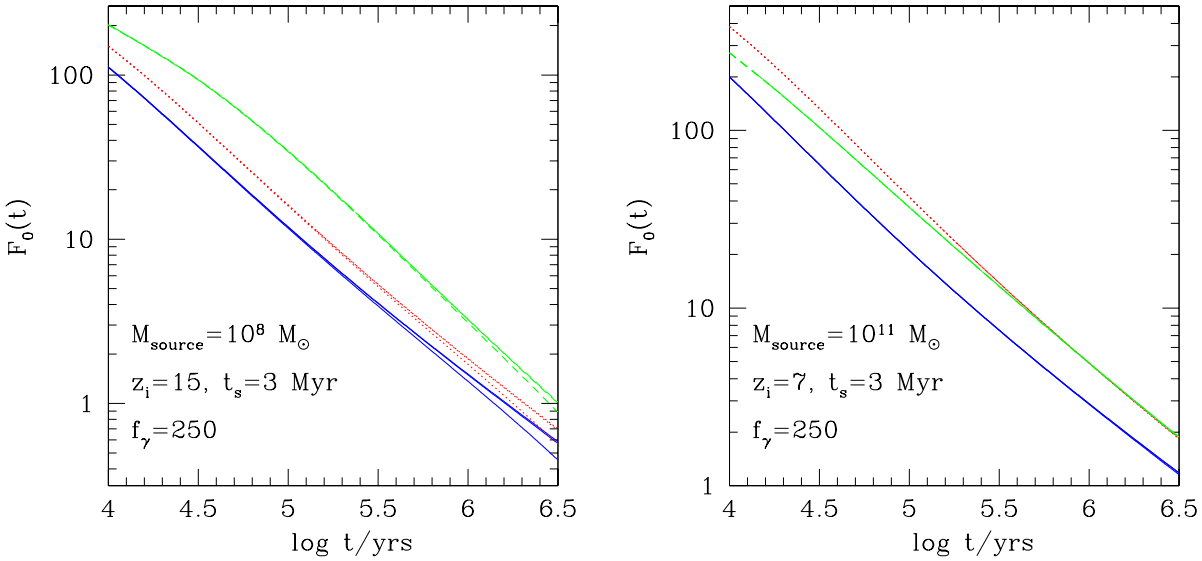

FIG. 6.— Evolution of the dimensionless ionizing photon flux $F_0(t)$ at the current position of the I-front. Same notation as in Fig. 4. Bottom set of (initially-overlapping) curves are for $C = 0$, middle set - for $C = 1$ and top set - for $C = 10$, respectively.(See the electronic edition of the Journal for the color version of this figure.)

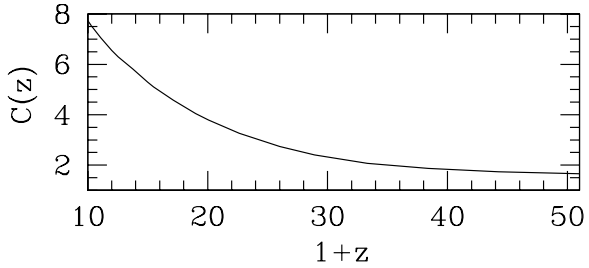

FIG. 7.— Evolution of the IGM clumping factor in ΛCDM from numerical N-body simulations, for the gas *outside* halos.

biased minihalos [as given by eq. (35)]. In Figure 4 we show the evolution of the ionized volume. All volumes are normalized to $V_{\rm max} = N_\gamma/n_H^0$, i.e. the volume ionized if there were no minihalos and no recombinations in the gas.

The increase of the clumping factor from $C = 1$ to $C = 10$ significantly decreases the maximum ionized volume achieved by the H II regions, with and without minihalos, especially at higher redshift, as shown for the $z = 15$ case in Figure 4. For similar reasons, H II regions around source halos in overdense areas of the IGM must also be smaller than those in the mean IGM. For $C = 0$ and no minihalos, $V_{\rm max}/V_0 = f_\gamma$, so $r_{\rm I,max}/r_0 = f_\gamma^{1/3}$. Since more realistic cases, with $C > 1$ and minihalos, all have $V_I < V_{\rm max}$, it must be true that $r_I/r_0 < f_\gamma^{1/3}$, in general. According to Figure 2, the overdensity $\delta_{\rm clump} > 1$ outside the source halo for all $r/r_0 \lesssim 20$, while $\delta_{\rm clump} > 2$ for all $r/r_o \lesssim 4$ (6), for source halos of mass 10^{11} (10^8) $M_\odot$. As such, the IGM recombination correction to the ionized volume at any epoch must be significantly enhanced by this local overdensity for any $f_\gamma \lesssim 1000$. In short, for a realistic range of f_γ values, cosmological H II regions from stellar sources are generally not larger than the infall regions associated with their source halos. This is true with and without minihalos.

Next we consider the effect of adding minihalos. According to Figure 4, for the $10^8 M_\odot$ source halo, the unbiased minihalo distribution decreases the ionized volume by $\sim 20\%$ compared to the no minihalos case, while when we account for the minihalo bias about the source, the ionized volume is decreased by a factor of 2 relative to the no minihalos case. For the $10^{11} M_\odot$ source halo, the net ionized volume when minihalos are present (biased or not) is about 65% of the volume in the case without minihalos.

In the top panel of Figure 5, we plot the factor $\beta_{\rm i}/\chi_{\rm eff}$ by which minihalo evaporation boosts the number of ionizing photons consumed at the I-front per atom that crosses the front (in the IGM and in minihalos combined). In the bottom panel of this figure, we plot the comoving (Eulerian) radius of the corresponding H II regions. For the $10^8 M_\odot$ source halo at $z_i = 15$, ignoring the minihalo bias (bottom lines) seriously underestimates the photon consumption by a factor of $\gtrsim 2$ as compared to the biased minihalos (top lines). Furthermore, the overall effect of adding minihalos is to increase the photon consumption by $\sim 100\%$. For the $10^{11} M_\odot$ halo at $z_i = 7$, there is a similar increase in the photon consumption, but little difference between the biased and unbiased results.

Finally we plot the dimensionless flux F_0 at the current position of the I-front, in Figure 6. This is important as a check of our assumptions, which incorporate simulation results for minihalo evaporation for a range of fluxes, $10^{-2} \leq F_0 \leq 10^3$. The value of F_0 has a significant impact on the ionizing photon consumption of minihalos, which is higher for higher values of F_0. In both cases, the flux starts fairly high ($F_0 \gtrsim 100$), but drops to $F_0 \sim 1$ by the time the source starts to fade. At first this drop is due mainly to geometric dilution, but later, recombinations in the ionized volume accelerate this decrease according to equation (29).

3. TOWARDS A MORE GLOBAL PICTURE

To construct models of the global reionization process, we first calculate the number density of source halos at each redshift based on the PS formalism. We then calculate the evolution of the H II region created by each source halo, as discussed in section §2.2 and §2.3. Finally, we add the volumes of all these H II regions. This gives the total ionized mass fraction at each redshift, according to

$$f_{I,M} = \int_{M_{\rm s,min}}^{\infty} dM \int_z^{\infty} dz' \frac{dn_{\rm s}(M,z')}{dMdz'} V_I(z,z',M,\dot{N}_\gamma), \qquad (39)$$

where $\frac{dn_{\rm s}(M,z')}{dMdz'}$ is the PS distribution of the source halos, and we assume here that source halos have masses $M_s \geq M_{\rm s,min} = M(10^4{\rm K})$, the mass of halos with $T_{\rm vir} = 10^4$ K. The universe is fully ionized when the H II regions overlap, which corresponds to $f_{I,M} = 1$.

3.1. *Time-Dependent Clumping Factor of IGM Outside Halos*

As in the individual-source results above, we calculate the evolution of the ionized mass fraction for the cases of no minihalos, unbiased minihalos, and biased minihalos, and for clumping factors of $C = 0, 1$ and 10. In addition, we consider the more realistic case of a clumping factor that evolves in time as more and more structure forms, which was obtained from numerical N-body simulations by the particle-particle/particle mesh (P^3M) method, with a computational box size of 1 comoving Mpc with 128^3 particles and 256^3 cells, corresponding to a particle mass of $2 \times 10^4 M_\odot$ (see Shapiro 2001 and Iliev et al. 2003 for details on the simulations). The result for the IGM clumping factor is plotted in Figure 7. This clumping factor excludes the matter in collapsed halos, since as we discussed above, these are self-shielded and we treat them separately. The evolution of this IGM clumping factor with redshift is well-fit by

$$C(z) = 17.6e^{-0.10z+0.0011z^2}. \qquad (40)$$

3.2. *The Global Consumption of Ionizing Photons During the Epoch of Reionization*

The reionization of the universe was complete when the volume of all the H II regions at some epoch equaled the total volume. We call that the epoch of overlap, at redshift $z_{\rm ov}$. Generalizing Shapiro & Giroux (1987) we define a useful dimensionless ratio of total number of ionizing photons emitted per hydrogen atom in the universe until overlap at $z = z_{\rm ov}$ given by,

$$\zeta_{\rm ov} = \frac{f_\gamma \Omega_b}{n_H^0 \mu m_p t_s} \int_\infty^{z_{\rm ov}} dz \int_{M_{\rm s,min}}^{\infty} M_s dM_s \int_{t(z)}^{t(z_{\rm ov})} dt' \frac{dn_{\rm x}^0(M_s,z')}{dM_s dz'} \frac{dz'}{dt'}, \qquad (41)$$

where $dn_{\rm x}^0(M,z)/dMdz$ is the comoving differential number density of the source halos of mass M formed at redshift z.

3.3. *Electron Scattering Optical Depth Through the Reionized Universe*

For any given reionization history, the mean optical depth along a line-of-sight between an observer at $z = 0$ and a redshift z due to Thomson scattering by free electrons in the post-recombination universe is given by

$$\tau_{\rm es}(z) = c\sigma_T \int_z^0 dz' n_e(z') \frac{dt}{dz'}, \qquad (42)$$

where $\sigma_T = 6.65 \times 10^{-25}{\rm cm}^2$ is the Thomson scattering cross-section, c is the speed of light, and $n_e(z)$ is the mean number density of free electrons at redshift z, given by

$$n_e(z) = n_{\rm e,0}(1+z)^3 f_{I,M}(z), \qquad (43)$$

where $f_{I,M}(z)$ is the ionized fraction of the IGM at redshift z, and $n_{\rm e,0} = n_H^0 \chi_{\rm eff}$. For comparison with the value of $\tau_{\rm es}$ between us

and the surface of last scattering inferred from measurements of the polarization of the CMB, we should evaluate $\tau_{\rm es}(z)$ at $z = z_{\rm rec}$, the redshift of recombination. For this paper we assume that He is ionized to He II at the same time as H is ionized. We make the reasonable approximation that $p = 2$ (1) in $\chi_{\rm eff}$ for $z \leq 3.5$ ($z > 3.5$). In fact, the reionization of helium to He III at $z \sim 3-4$, inferred from observations of quasar absorption spectra, has only a small effect on the total electron-scattering optical depth and can be ignored for most purposes. In the case of $f_{I,M}$ = const between us and redshift z (e.g. for an IGM fully ionized and free of minihalos since $z_{\rm ov}$, $f_{I,M} = 1$ for $z \leq z_{\rm ov}$), the integral in equation (42) has a closed analytical form

$$\tau_{\rm es}(z) = \frac{2c\sigma_T \Omega_b \rho_{\rm crit,0}}{3H_0 \mu_H m_p \Omega_0} f_{I,M} \chi_{\rm eff} \left\{ [\Omega_0 (1+z)^3 + \Omega_\Lambda]^{1/2} - 1 \right\}, \quad (44)$$

where $\mu_H = 1 + 4A({\rm He}) = 1.32$, the mean molecular weight per H atom. For $f_{\rm I,M} = 1(0)$ for $z \leq z_{\rm ov}$ ($z > z_{\rm ov}$), $\tau_{\rm es} \geq 0.04$ for $z_{\rm ov} \geq 6$.

4. GLOBAL REIONIZATION MODELS: RESULTS AND CONCLUSIONS

4.1. *Fiducial Model*

We first consider a fiducial model, Case A, that assumes that the sources are Pop. II starbursts, with $f_\gamma = 250$ and a lifetime of $t_s = 3$ Myr. The evolution of the ionized mass fractions for Case A, with and without minihalos and IGM clumping, is shown in Figure 8. At $z \gtrsim 15$ there are very few minihalos. Thus in the $C = 0$ case, the no-minihalos model and the model with unbiased minihalos are almost equivalent. The few minihalos that do exist at such early times, however, are highly biased towards the sources, giving rise to a substantial difference between the biased and unbiased models. Similar trends are visible in the $C = 1$ case with minihalos having an appreciable impact only in the biased case. On the other hand, in the $C(z)$ model, recombinations in non-virialized structures slow reionization to the point where a significant average minihalo collapse fraction builds up, giving rise to a shift (i.e. delay) of $\Delta z \sim 2$ between the no minihalos and unbiased minihalo models. In this case, the minihalo correction increases with time relative to the case without minihalos, as expected since the unbiased $f_{\rm coll,MH}$ grows with time. This has the effect of slowing the rate of increase of the ionized volume more and more over time. This trend would help reconcile an early onset of reionization with a late epoch of overlap. When minihalo bias is taken into account, however, the minihalo correction is just as large at early times as at late times. At late times the biased and unbiased minihalo curves almost converge, since the clustering of small objects is very weak at these times and bias has a minimal effect.

The results for $z_{\rm ov}$, $\zeta_{\rm ov}$ and the net $\tau_{\rm es}$, $\tau_{\rm es}(z_{\rm rec})$, for our fiducial model, Case A, are shown in Table 1 and in Figure 9 for $\tau_{\rm es}(z)$. When there are no minihalos and no recombinations in the IGM, $z_{\rm ov} = 15.2$ and $\tau_{\rm es} = 0.186$, which requires just one photon per atom (i.e. $\zeta_{\rm ov} = 1$). The presence of minihalos by themselves delays overlap until $z_{\rm ov} = 14$, while increasing the global photon consumption by a factor of ~ 2 and decreasing the optical depth to 0.169. The IGM clumping by itself delays overlap until $z_{\rm ov} = 8.1(9.5)$ for $C = 10[C(z)]$, increasing the global photon consumption to 23(14) and decreasing $\tau_{\rm es}$ to 0.090(0.114). When the effects of both minihalos and redshift-dependent IGM clumping are included, overlap is further delayed until $z_{\rm ov} = 7.2$, in rough consistency with the results from the Gunn-Peterson trough observations, while the electron-scattering optical depth decreases to 0.089, somewhat below the $1-\sigma$ WMAP limit, and the global ionizing photon consumption rises to $\zeta_{\rm ov} = 33$.

4.2. *Impact of Model Uncertainties and Discussion*

In order to estimate the effects of small-scale structure under different assumptions, we consider several cases in addition to our fiducial model (Case A). Case B is the same as our fiducial model, but assumes that the sources are longer-lived, with $t_s = 100$ Myr. Case C is also the same as our fiducial model, but assumes that the formation times of the minihalos are distributed in redshift, by replacing equation (32) with equation (33) for unbiased minihalos and equation (35) with equation (36) for biased minihalos as discussed in sections § 2.2.1 and § 2.2.2. Cases D, E and F are like Case A, except with $f_\gamma = 40$ (Case D), 150 (Case E) and 500 (Case F). Finally, Case G assumes Pop. III sources with a $t_s = 3$ Myr lifetime and $f_\gamma = 250$.

The values of $z_{\rm ov}$, $\zeta_{\rm ov}$ and $\tau_{\rm es}$ for each of these cases are summarized in Table 1. In all cases the clumping of the IGM gas a strong effect on the duration of reionization by significantly increasing recombination rates and the ionized photon consumption. Thus increasing C from 1 (no clumping) to 10 delays the overlap by $\Delta z \approx 4-6$ and increases the global ionizing photon consumption $\zeta_{\rm ov}$ by a significant factor, between 6 and 17. The electron-scattering optical depth $\tau_{\rm es}$ decreases correspondingly, from $\sim 0.11-0.17$ (consistent with current WMAP limits) for $C = 1$, to $\sim 0.04-0.1$ for $C = 10$. Interestingly, the cases with evolving clumping factor $C(z)$ yield epochs of overlap similar to those of the $C = 10$ cases, while at the same time noticeably increasing $\tau_{\rm es}$, by $\Delta\tau_{\rm es} \sim 0.02$ to $\sim 0.09-0.11$, reaching better agreement with the observational limits from WMAP.

The presence of minihalos additionally delays reionization, by up to $\Delta z \approx 2.5$. This effect is strongest for short-lived sources, and almost disappears for very long-lived sources (Case B). This is because in the long-lived case, the same total number of photons are produced over a longer time, and thus the typical flux responsible for evaporating minihalos is lower, leading to more efficient photoevaporation in terms of ionizing photon consumption. Similarly, in the short-lived case, the photon consumption by minihalos typically raises the global photon consumption per atom until overlap, $\zeta_{\rm ov}$, by a factor of ~ 2, while in Case B, the $\zeta_{\rm ov}$ increases range from 10 to 60%, depending on the clumping factor.

Turning to the question of our assumptions about minihalo formation times, we find that the differences between cases A and C are negligible in all cases. Thus we can generally assume that the minihalos just formed at the redshift of consideration as opposed to formation times that are distributed in redshift.

What is the effect of varying the efficiency for ionizing photon release? In Case D, in which reionization is caused by Pop. II sources with $f_\gamma = 40$, we find that overlap is achieved before $z = 6$ only when there is no gas clumping ($C = 1$), even if no minihalos are present. Hence, f_γ (which depends upon the assumed photon production per stellar baryon, star-formation efficiency per halo baryon and the ionizing photon escape fraction) should be significantly larger than this assumed value (e.g. by replacing the Salpeter IMF by a top-heavy one). For $f_\gamma = 150$ (Case E), the values of $z_{\rm ov}$ and $\tau_{\rm es}$ without minihalos are essentially equivalent to those in our fiducial Case A when biased minihalos are included, for all values of the clumping factor. The quantity $\zeta_{\rm ov}$ is smaller in Case E than in Case A, however.

Since Case A has too small a value of $\tau_{\rm es}$ to satisfy the

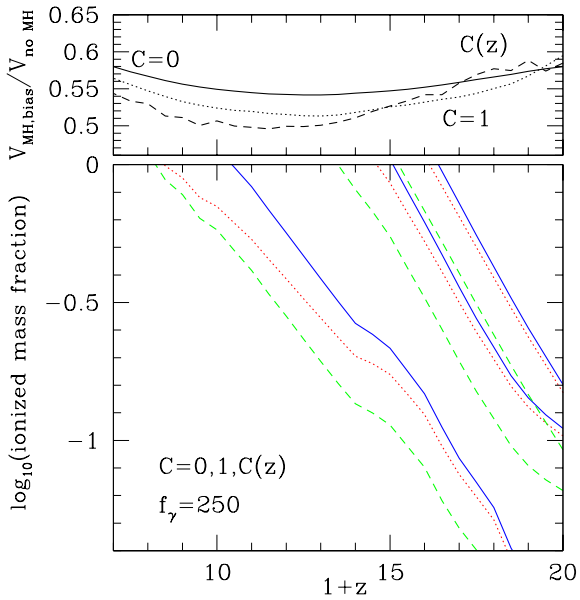

FIG. 8.— Global reionization. Sources with f_γ = 250 and lifetime of t_s = 3 Myr (Case A) are assumed. (bottom panel) Decimal logarithm of ionized mass (or Lagrangian volume) fractions (i.e. 0 corresponds to overlap) for the cases of no minihalos (solid), unbiased minihalos (dotted), and biased minihalos (dashed) for IGM clumping factors (top to bottom in each case) C = 0, 1, and C(z) (clumped IGM). (upper panel) Ratios of the ionized volume fractions in the presence of *biased* minihalos and with no minihalos for C = 0, 1 and z-dependent.(See the electronic edition of the Journal for the color version of this figure.)

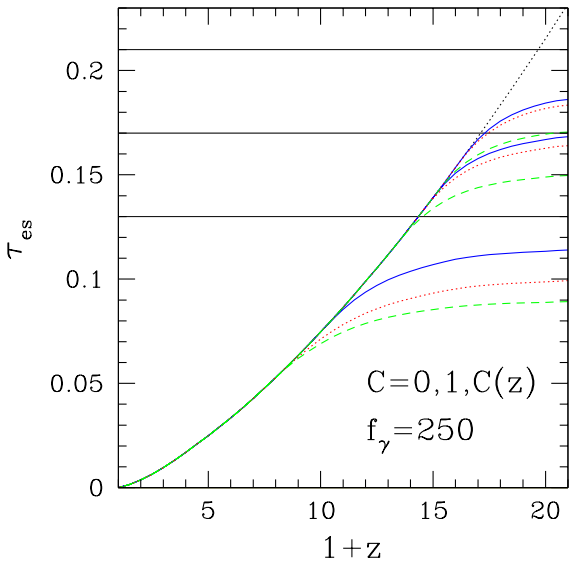

FIG. 9.— Global reionization. Integrated optical depth due to electron scattering $\tau_{\rm es}$ vs. redshift. Same notation as in Fig. 8. Top (dotted) curve shows the optical depth produced assuming complete ionization out to the corresponding redshift. Horizontal lines indicate the best-fit and $1-\sigma$ uncertainties of the first-year WMAP result, $\tau_{\rm es} = 0.17 \pm 0.04$. (See the electronic edition of the Journal for the color version of this figure.)

TABLE 1

GLOBAL REIONIZATION RESULTS FOR IONIZING PHOTON CONSUMPTION, ζ_{ov} OVERLAP EPOCH, z_{ov} [a] , AND ELECTRON SCATTERING OPTICAL DEPTH, τ.

No MH			$C = 0$			$C = 1$			$C = 10$			$C = C(z)$	
Case	f_γ	ζ_{ov}	z_{ov}	τ_{es}	ζ_{ov}	z_{ov}	τ	ζ_{ov}	z_{ov}	τ_{es}	ζ_{ov}	z_{ov}	τ_{es}
A	250	1	15.4	0.186	2.1	14.2	0.168	23	8.1	0.089	14	9.5	0.114
B	250,long life	1	13.6	0.157	1.8	13	0.144	13	9	0.096	9	9.8	0.108
C	250,z-distr.	1	15.4	0.186	2	14.2	0.168	24.5	8.1	0.090	15	9.4	0.114
D	40	1	11.3	0.137	2.7	9.3	0.107	...	...	0.045	...	...	0.048
E	150	1	14.4	0.173	2.3	12.7	0.151	24	6.5	0.072	21	7.0	0.088
F	500	1	17	0.205	2.	15.5	0.192	20	10.5	0.118	10.0	12	0.151
G	250	1	15.4	0.186	2.1	14.2	0.168	23	8.1	0.089	14	9.5	0.114
MH, no bias													
A	250	1.2	15	0.183	2.5	13.6	0.164	39	6.7	0.077	30	7.5	0.099
B	250,long life	1.2	13.5	0.155	2	12.5	0.142	14	9	0.096	9	9.8	0.107
C	250,z-distr.	1.2	15	0.183	2.6	13.7	0.163	43	6.6	0.076	34	7	0.095
D	40	1.3	11	0.131	4.4	8	0.095	...	...	0.043	...	...	0.044
E	150	1.2	14	0.169	3	12	0.144	34	5.5	0.059	34	5.5	0.072
F	500	1.2	16.5	0.203	2.1	15.5	0.189	30	9.5	0.108	16.0	11	0.141
G	250	1.1	15.2	0.185	2.2	14	0.166	31	7.3	0.082	22	8.3	0.106
MH, w/bias													
A	250	1.9	14	0.169	4.3	12.4	0.148	40	6.6	0.072	33	7.2	0.089
B	250,long life	1.6	13	0.148	2.3	12.3	0.138	14	9	0.095	10	9.7	0.106
C	250,z-distr.	2.1	14	0.169	4.5	12.4	0.148	44	6.6	0.072	35	7	0.087
D	40	2.0	10	0.117	5.1	7.5	0.085	...	...	0.043	...	...	0.044
E	150	2.0	13	0.154	4.6	11.0	0.129	34	5.5	0.057	34	5.5	0.067
F	500	1.8	15.3	0.192	3.4	14.5	0.176	37	9	0.100	22.0	10	0.126
G	250	1.5	14.7	0.177	3.2	13	0.157	32	7.2	0.079	24.5	8	0.099

[a]When no value of z_{ov} is given, overlap was not achieved by $z = 5.5$.

WMAP constraint, we consider a case with higher efficiency for photon release $f_\gamma = 500$ (Case F), to increase τ_{es} by making reionization earlier. With evolving clumping factor $C(z)$ and biased minihalos, Case F results in $\tau_{es} = 0.126$, which is marginally consistent with the 1-σ WMAP constraint, but $z_{ov} = 10$, too early to match quasar observations.

Finally, we illustrate the difference between Pop. II and Pop. III ionizing source spectra in Case G, for which massive Pop. III stars provide $f_\gamma = 250$. The only difference between Case G and Case A is the source spectral shape, which results in somewhat more efficient evaporation of the minihalos. Hence, overlap is slightly earlier, at $z_{ov} = 8$, and ζ_{ov} is a bit smaller, at 25, while τ_{es} is a bit higher, at $\tau_{es} \simeq 0.1$, so there is still not a good agreement with both the quasar and CMB constraints. If we reduce f_γ somewhat, for this Pop. III case, the overlap redshift would drop, but so would τ_{es}, so it would not help to match these observations simultaneously. We conclude from this that this problem is not very sensitive to our choice of source spectrum.

It would appear then that our fiducial model Case A with minihalos is the best candidate for helping to resolve QSO constraints on z_{ov} with the WMAP measurements of τ_{es}. For although the model still falls short of reproducing the observed τ_{es}, minihalos nevertheless form *on average* in small numbers at early times and in large numbers at late times, thereby extending reionization and accumulating scattering optical depth before overlap. However, this behavior changes dramatically if one accounts for the strong clustering of high-z minihalos. As shown in Figure 3, the minihalo collapsed fraction in the neighborhood of the typical source halos is significantly higher than the spatially-averaged collapsed fraction of minihalos at the same epoch. Hence, although the total number of minihalos increases with time, the number *around sources* remains largely fixed, pushing the entire process of reionization to later times, without significantly extending its duration.

This can be understood from our analytical solution for an H II region in a uniform IGM for a steady source, discussed in § 2, if we assume that β_i is independent of time. In that case, the H II region volume $V(t)$ in the presence of minihalos equals the volume it would have had at some time t in the absence of minihalos, at a later time $t' = t(\beta_i/\chi_{\rm eff})$. This argument shows that the rate of growth of the ionized volume, dV_I/dt, decreases in the presence of minihalos by the factor $\beta_i/\chi_{\rm eff}$. This tilts the curve of the rise of the mean ionized fraction of the IGM with time to a flatter slope, which has the effect of extending the reionization epoch and delaying overlap.

In order to reconcile the late epoch of overlap implied by observations of high-z QSO's with the early start of reionization implied by WMAP polarization results, we would like the rise of the ionized volume to be more rapid at early times than at late times. This is the effect which *unbiased* minihalos have, according to the curves in Figure 8, because the average of the factor $\beta_i/\chi_{\rm eff}$ increases with time in that case as the average collapsed fraction of minihalos grows. However, when minihalo bias is taken into account, the effective average correction factor $\beta_i/\chi_{\rm eff}$ remains roughly constant in time, thereby reducing dV_I/dt by the same factor at all times, instead of a factor which increases over time as required to reconcile the two observations. Thus although minihalos have a large effect on ζ_{ov}, they do not help to reconcile the WMAP and high-redshift QSO results. Instead they essentially act as local screens that reduce the effective number of photons that can impact the IGM at any given redshift, given a choice of f_γ. A similar slow-down of the growth of the ionized volume would result if we neglected the minihalos but adopted a smaller efficiency for the release of ionizing photons by the source halos, instead, as seen by com-

paring Cases A and E.

The evolving clumping factor, on the other hand, does have the desired effect of not only extending reionization, but also producing significant ionized volume early on, when the IGM clumping is low. This serves to bring the electron scattering optical depth closer to the WMAP constraint, while also delaying overlap.

We have demonstrated here that small-scale structure, which has generally been neglected by previous treatments of reionization, can have a substantial effect on the duration and epoch of completion of reionization. In the future we can use the approach presented here to explore reionization under more complex set of assumptions, allowing for the dependence of the ionizing photon production efficiency and escape fraction on time and halo mass and for the clustering of source halos, for instance. Our current results suggest, for example, that an efficiency parameter f_γ which decreases in time or with increasing source halo mass, may cause the rise of ionized volume to decelerate over time, which would help to explain observations of early reionization onset and late epoch of overlap.

We are grateful to Hugo Martel for his help with the N-body simulation data and clumping factor determination. We thank Andrea Ferrara for helpful comments during the preparation of this manuscript. ITI was supported in part by the Research and Training Network "The Physics of the Intergalactic Medium" established by the European Community under the contract HPRN-CT2000-00126. ES was supported by an NSF Math and Physical Sciences Distinguished International Postdoctoral Research (NFS MPS-DRF) fellowship during part of this investigation; his research was also supported by the National Science Foundation under grant PHY99-07949. This work was partially supported by NASA grants NAG5-10825 and NNG04G177G and Texas Advanced Research Program grant 3658-0624-1999 to PRS. The final draft of this paper was completed during visits by ES to CITA and of PRS and ITI to the KITP at UCSB as part of the 2004 Galaxy-IGM Interactions Program.

REFERENCES

Barkana, R., & Loeb, A. 2002, ApJ, 578, 1
Barkana, R., & Loeb, A. 2004, ApJ, 609, 474
Barkana, R. 2004, MNRAS, 347, 59
Cen, R. 2003, ApJ, 591, 12
Chen, X., & Kamionkowski, M. 2004, Phys. Rev. D, 70, 3502
Chiu, W. A., Fan, X., & Ostriker, J. P. 2003, ApJ, 599, 759
Ciardi, B., Ferrara, A., Governato, F., & Jenkins, A. 2000, MNRAS, 314, 611
Ciardi, B., Ferrara, A., & White, S. D. M. 2003, MNRAS, 344, 7
Ciardi, B., Stoehr, F., & White, S. D. M. 2003, MNRAS, 343, 1101
Eisenstein, D. J. & Hu, W. 1999, ApJ, 511, 5
Eke, V. R., Cole, S., & Frenk, C. S. 1996, MNRAS, 282, 263
Fan, X., et al. 2004, AJ, 128, 515
Gnedin, N. Y. 2000, ApJ, 535, 530
Hansen, S., & Haiman, Z. 2004, ApJ, 600, 26
Haiman, Z., Abel, T., Rees, M., 2000, ApJ, 534, 511
Haiman, Z., Abel, T., Madau, P., 2001, ApJ, 551, 599
Haiman, Z., & Holder, G. P. 2003, ApJ, 595, 1
Haiman, Z., Rees, M., & Loeb, A. 1997, ApJ, 476, 458 (erratum 484, 985)
Heckman, T. M., Sembach, K. R., Meurer, G. R., Leitherer, C., Calzetti, D., Martin, C. L. 2001, ApJ, 558, 56
Iliev, I. T., Scannapieco, E., Martel, H., & Shapiro, P. R. 2003, MNRAS, 341, 81
Iliev, I. T., Shapiro, P. R., Raga, A. C. 2004, submitted to MNRAS (astro-ph/0408408)
Kitayama, T., & Suto, Y. 1996, MNRAS, 280, 638
Kogut, A. et al. 2003, ApJS, 148, 161
Lacey, C. & Cole, S. 1993, MNRAS, 262, 627
Leitherer, C., Ferguson, H. C., Heckman, T. M., Lowenthal, J. D. 1995, ApJ, 454, 19L
Leitherer, C. et al. 1999, ApJS, 123, 3
Loeb, A., & Eisenstin, D. J. 1995, ApJ, 448, L17
Miralda-Escudé, J., Haehnelt, M., & Rees, M. J. 2000, ApJ, 530, 1
Mo, H. J., & White, S. D. M. 1996, MNRAS, 282, 347
Onken, C. A., & Miralda-Escudé, J. 2004 ApJ, 610, 1
Peebles, P. J. E. 1980, The Large-Scale Structure of the Universe, Princeton University Press, Princeton, NJ
Perlmutter, S., et al. 1999, ApJ, 517, 565
Porciani, C., Matarrese, S., Lucchin, F., & Catelan, P. 1998, MNRAS, 298, 1097
Press, W. H., & Schechter, P. 1974, ApJ, 187, 425 (PS)
Razoumov, A. O., Norman, M. L., Abel, T. & Scott, D. 2002, ApJ, 572, 695
Ricotti, M.,& Shull, J. M. 2000, ApJ, 542, 548
Ricotti, M., Gnedin, N., & Shull, J. M. 2002, ApJ, 575, 33
Scannapieco, E., & Barkana, R. 2002, ApJ, 571, 585
Scannapieco, E. & Schneider, R., & Ferrara, A. 2003, ApJ, 589, 35
Schaerer, D. 2002, A&A, 382, 28
Shapiro, P. R. 1986, PASP, 98, 1014
Shapiro, P. R. 2001, in Proceedings of the 20th Texas Symposium on Relativistic Astrophysics and Cosmology, eds. H. Martel and J. C. Wheeler, (AIP Conference Series), pp. 219-232
Shapiro, P. R., & Giroux, M. L. 1987, ApJ, 321, 107L
Shapiro, P. R., Iliev, I. T., Raga, A. C., 2004, MNRAS, 348, 753
Shapiro, P. R., Iliev, I. T., Raga, A. C., & Martel, H. 2003 in *The Emergence of Cosmic Structure*, eds. Holt, S. S. & Reynolds, C. S. (AIP Conf. Proc. 666), pp. 89-92
Sokasian, A., Yoshida, N., Abel, T., Hernquist, L., Springel, V. 2004, MNRAS, 350, 47
Spergel, D. N., et al. 2003, ApJS, 148, 175
Steidel, C. C., Pettini, M., Adelberger, K. L. 2001, ApJ, 546, 665
Tan, J. C., & McKee, C. F. 2001 in *Starburst Galaxies: Near and Far*, eds. L. Tacconi and D. Lutz. Heidelberg: Springer-Verlag, p. 188 (astro-ph/0012005)
Tumlinson, J., Venkatesan, A., & Shull, J. M. 2004, ApJ, 612, 602
Venkatesan, A., Tumlinson, J., & Shull, J. M. 2003, ApJ, 584, 621
White, R. L., Becker, R. H., Fan, X., Strauss, M. A. 2003,AJ, 126, 1
Wyithe, J. S. B., & Loeb, A. 2003, ApJ, 586, 693